



Cite this: *Phys. Chem. Chem. Phys.*, 2016, 18, 21102

## Planar vs. three-dimensional $X_6^{2-}$ , $X_2Y_4^{2-}$ , and $X_3Y_3^{2-}$ ( $X, Y = B, Al, Ga$ ) metal clusters: an analysis of their relative energies through the turn-upside-down approach<sup>†‡</sup>

Ouissam El Bakouri,<sup>a</sup> Miquel Solà\*<sup>a</sup> and Jordi Poater\*<sup>bcd</sup>

Despite the fact that B and Al belong to the same group 13 elements, the  $B_6^{2-}$  cluster prefers the planar  $D_{2h}$  geometry, whereas  $Al_6^{2-}$  favours the  $O_h$  structure. In this work, we analyse the origin of the relative stability of  $D_{2h}$  and  $O_h$  forms in these clusters by means of energy decomposition analysis based on the turn-upside-down approach. Our results show that what causes the different trends observed is the orbital interaction term, which combined with the electrostatic component do ( $Al_6^{2-}$  and  $Ga_6^{2-}$ ) or do not ( $B_6^{2-}$ ) compensate the higher Pauli repulsion of the  $O_h$  form. Analysing the orbital interaction term in more detail, we find that the preference of  $B_6^{2-}$  for the planar  $D_{2h}$  form has to be attributed to two particular molecular orbital interactions. Our results are in line with a dominant delocalisation force in Al clusters and the preference for more localised bonding in B metal clusters. For mixed clusters, we have found that those with more than two B atoms prefer the planar structure for the same reasons as for  $B_6^{2-}$ .

Received 18th February 2016,  
Accepted 11th March 2016

DOI: 10.1039/c6cp01109h

[www.rsc.org/pccp](http://www.rsc.org/pccp)

### Introduction

The electronic distribution of nanosized molecular clusters can be very different from that of the bulk state.<sup>1</sup> In fact, metals can exhibit isolating behaviour when reduced to small particles. Since the electronic properties of nanoparticles are quite different from those of the bulk, molecular clusters are expected to have a variety of electronic applications, such as single-electron transistors, diodes, and quantum dots.<sup>2-4</sup> The properties of clusters are profoundly affected by the type of bonding they have. For some of these clusters one can expect an intermediate situation between covalent and metallic bonding. As modern technologies evolve towards the nanoscale, it becomes more

important to have a more precise understanding of the bonding in these species to better tune their properties.

Among clusters, those made by group 13 atoms are particularly important.<sup>5</sup> Both B and Al belong to the same group 13, and thus present a similar electronic structure,  $[He]2s^22p^1$  and  $[Ne]3s^23p^1$ , respectively. However, when they form small clusters, B clusters adopt a planar conformation as the equilibrium structure;<sup>6-9</sup> whereas Al clusters present a three-dimensional (3D) closed shape.<sup>10-13</sup> The most relevant examples are  $B_6^{2-}$  and  $Al_6^{2-}$  clusters, which were obtained experimentally as lithium salts in the form of  $LiB_6^-$  and  $LiAl_6^-$ .<sup>14-16</sup>  $B_6^{2-}$  adopts a planar  $D_{2h}$  geometry in its low-lying singlet state, whereas the  $Al_6^{2-}$  cluster is octahedral. Both shapes of the metal clusters are kept when lithium salts are formed.

The chemical bonding of  $B_6^{2-}$  and  $Al_6^{2-}$  has been widely analysed in previous studies.<sup>14,17,18</sup> In particular, Alexandrova *et al.*<sup>18</sup> highlighted the fact that  $B_6^{2-}$  is able to 2s-2p hybridize and to form 2-center-2-electron (2c-2e) B-B covalent localised bonds. On the other hand, 3s-3p hybridisation in the  $Al_6^{2-}$  cluster is more difficult due to larger s-p energy separation, which hampers the formation of directional covalent Al-Al bonds.<sup>19</sup> In this case, bonding comes from the combination of radial and tangential p-orbitals that result in extensive delocalisation.<sup>20</sup> Indeed, the  $Al_6^{2-}$  cluster displays octahedral aromaticity,<sup>14,21</sup> whereas planar  $D_{2h}$   $B_6^{2-}$  is considered  $\sigma$ - and  $\pi$ -antiaromatic.<sup>17,18,22,23</sup> Thus, as pointed out by Alexandrova *et al.*,<sup>18,24-26</sup> covalent and delocalised bonding shows opposite

<sup>a</sup> Institut de Química Computacional i Catalisi (IQCC) and Departament de Química, Universitat de Girona, Campus Montilivi, 17071 Girona, Catalonia, Spain. E-mail: miquel.sola@udg.edu

<sup>b</sup> Departament de Química Inorgànica i Orgànica & Institut de Química Teòrica i Computacional (IQTCB), Universitat de Barcelona, Martí i Franquès 11-11, 08028 Barcelona, Catalonia, Spain. E-mail: jordi.poater@gmail.com

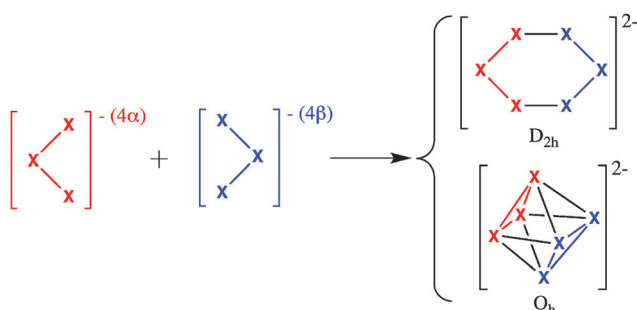
<sup>c</sup> Department of Theoretical Chemistry and Amsterdam Center for Multiscale Modeling, Vrije Universiteit Amsterdam, De Boelelaan 1083, NL-1081HV Amsterdam, The Netherlands

<sup>d</sup> Institut Català de Recerca i Estudis Avançats (ICREA), Pg. Lluís Companys 23, 08010 Barcelona, Catalonia, Spain

† This work is dedicated to Prof. Evert Jan Baerends as a proof of our admiration for his brilliant contributions to chemistry and of our gratitude for helping us to understand chemistry better.

‡ Electronic supplementary information (ESI) available. See DOI: 10.1039/c6cp01109h





Scheme 1  $D_{2h}$  and  $O_h$  structures of  $X_6^{2-}$  can be formed from  $C_{2v} X_3^-$  fragments.

effects in determining the molecular structure of many clusters. Huynh and Alexandrova analysed the whole series  $B_n Al_{6-n}^{2-}$  ( $n = 0-6$ ), from  $B_6^{2-}$  till  $Al_6^{2-}$  by substituting one B by Al each time, concluding that covalent bonding is a resilient effect that governs the cluster shape more than delocalisation does. Indeed, the planar structure of  $B_6^{2-}$  persists until  $n = 5$ , the reason being the strong tendency to form 2c-2e B-B bonds in case the cluster contains two or more B atoms.<sup>18</sup> Similar results were reported by Fowler and Ugalde in larger clusters of group 13. In particular, these authors found that  $B_{13}^+$  prefers a planar conformation<sup>27</sup> in contrast to  $Al_{13}^-$ ,<sup>28</sup> which adopts an icosahedral geometry. Interestingly, in *clos*o boranes and substituted related species, like  $B_6H_6^{2-}$  or  $B_{12}I_{12}^{2-}$ , the delocalised 3D structure is preferred. However, successive stripping of iodine in  $B_{12}I_{12}^{2-}$  leads to a  $B_{12}$  planar structure with some localised 2c-2e B-B bonds.<sup>29,30</sup> Similarly, for  $B_6H_n^-$  clusters, the clusters are planar for  $n \leq 3$  and become tridimensional for  $n \geq 4$ .<sup>31</sup>

As can be seen in Scheme 1, both 2D  $D_{2h}$  planar and 3D  $O_h$  geometries for  $X_6^{2-}$  ( $X = B, Al$ ) can be obtained joining the same two  $X_3^-$  cluster fragments.<sup>14,17</sup> Therefore,  $X_6^{2-}$  species in  $D_{2h}$  and  $O_h$  geometries are particularly suitable for an energy decomposition analysis (EDA)<sup>32-35</sup> based on the turn-upside-down approach.<sup>36-39</sup> In this approach, two different isomers are formed from the same fragments and the bonding energy is decomposed into different physically meaningful components using an EDA. Differences in the energy components explain the reasons for the higher stability of the most stable isomer. For instance, using this method we provided an explanation of why the cubic isomer of  $T_d$  geometry is more stable than the ring structure with  $D_{4h}$  symmetry for  $(MX)_4$  tetramers ( $X = H, F, Cl, Br$ , and I) if M is an alkali metal and the other way round if M belongs to group 11 transition metals.<sup>38</sup> Therefore, the application of this type of analysis to  $B_6^{2-}$  and  $Al_6^{2-}$  clusters will disclose the factors that make the planar  $D_{2h}$  structure more stable for boron and the octahedral one for aluminium. As said before, boron clusters favour localised covalent bonds whereas aluminium clusters prefer a more delocalised bonding. With the present analysis, we aim to provide a more detailed picture of the reasons for the observed differences. The analysis will be first applied to the above referred  $B_6^{2-}$  and  $Al_6^{2-}$  clusters, and then further complemented with  $Ga_6^{2-}$ . Finally,  $X_2Y_4^{2-}$  and  $X_3Y_3^{2-}$  ( $X = B, Al, Ga$ ) mixed clusters in their distorted  $D_{2h}$  planar and 3D  $D_{4h}$  geometries will also be discussed.

## Computational methods

All Density Functional Theory (DFT) calculations were performed using the Amsterdam Density Functional (ADF) program.<sup>40</sup> The molecular orbitals (MOs) were expanded in a large uncontracted set of Slater type orbitals (STOs) of triple- $\zeta$  quality for all atoms (TZ2P basis set). The 1s core electrons of boron, 1s-2p of aluminium, and 1s-3p of gallium were treated by the frozen core approximation. Energies and gradients were computed using the local density approximation (Slater exchange and VWN correlation) with non-local corrections for exchange (Becke88) and correlation (Lee-Yang-Parr 1988) included self-consistently (*i.e.* the BLYP functional). D3(BJ) dispersion corrections by Grimme were also included in the functional (*i.e.* BLYP-D3(BJ) functional).<sup>41-44</sup> Analytical Hessians were computed to confirm the nature of the located minima at the same level of theory.

Relative energies between the planar and 3D species were also calculated using the Gaussian 09 program<sup>45</sup> at the coupled cluster level<sup>46</sup> with single and double excitation (CCSD)<sup>47</sup> and with triple excitation treated perturbatively (CCSD(T))<sup>48</sup> using Dunning's correlation consistent augmented triple- $\zeta$  (aug-cc-pVTZ)<sup>49,50</sup> at optimised BLYP-D3(BJ)/TZ2P molecular geometries.

The bonding energy corresponding to the formation of  $X_6^{2-}$  for both  $D_{2h}$  and  $O_h$  symmetries from two anionic quintet tetraradicals, fragment 1 ( $\alpha\alpha\alpha\alpha$ ) + fragment 2 ( $\beta\beta\beta\beta$ ) (see Scheme 1), is made up of two major components (eqn (1)):

$$\Delta E = \Delta E_{\text{dist}} + \Delta E_{\text{int}} \quad (1)$$

In this formula, the distortion energy  $\Delta E_{\text{dist}}$  is the amount of energy required to deform the separated tetraradical fragments in their quintet state from their equilibrium structure to the geometry that they acquire in the metal cluster. The interaction energy  $\Delta E_{\text{int}}$  corresponds to the actual energy change when the prepared fragments are combined to form the overall molecule. It is analysed in the framework of the Kohn-Sham MO model using a Morokuma-type decomposition<sup>32-35</sup> of the bonding energy into electrostatic interaction, exchange (or Pauli) repulsion, orbital interactions, and dispersion forces (eqn (2)).

$$\Delta E_{\text{int}} = \Delta V_{\text{elstat}} + \Delta E_{\text{Pauli}} + \Delta E_{\text{oi}} + \Delta E_{\text{disp}} \quad (2)$$

The term  $\Delta V_{\text{elstat}}$  corresponds to the classical electrostatic interaction between the unperturbed charge distributions of the prepared (*i.e.* deformed) fragments and is usually attractive. The Pauli repulsion  $\Delta E_{\text{Pauli}}$  comprises the destabilizing interactions between occupied MOs. It arises as the energy change associated with going from the superposition of the unperturbed electron densities of the two fragments to the wavefunction  $\Psi^0 = NA [\Psi_{\text{fragment1}}^{4\alpha} \Psi_{\text{fragment2}}^{4\beta}]$ , which properly obeys the Pauli principle through explicit antisymmetrisation ( $A$  operator) and renormalisation ( $N$  constant) of the product of fragment wavefunctions. It comprises four-electron destabilizing interactions between occupied MOs and is responsible for steric repulsion. The orbital interaction  $\Delta E_{\text{oi}}$  is the change in energy from  $\Psi^0$  to the final, fully converged wavefunction  $\Psi_{\text{SCF}}$  of the system. The orbital interactions account for charge transfer (*i.e.*, donor-acceptor interactions between occupied orbitals on one fragment with



unoccupied orbitals of the other, including the HOMO–LUMO interactions) and polarization (empty – occupied orbital mixing on one fragment due to the presence of another fragment). Finally, the  $\Delta E_{\text{disp}}$  term takes into account the interactions which are due to dispersion forces.

In bond-energy decomposition,<sup>51–53</sup> open-shell fragments were treated with spin-unrestricted formalism but, for technical reasons, spin-polarisation was not included. This error causes the studied bond to become in the order of a few  $\text{kcal mol}^{-1}$  too strong. To facilitate a straightforward comparison, the EDA results were scaled to match exactly the regular bond energies (the correction factor is consistently in the range 0.97–0.98 in all model systems and does therefore not affect trends). A similar scheme based on the same EDA approach was used by Frenking and coworkers<sup>54,55</sup> and by some of us<sup>36,37,56</sup> to estimate the strength of  $\pi$ -cyclic conjugation in typical (anti)-aromatic organic compounds and in metallaabenzenes and metallacyclopentadienes.

Let us mention here that, as already mentioned in the introduction, some of the analysed metal clusters exist experimentally as lithium salts.<sup>14–16</sup> On the other hand, these dianionic systems are unstable against the ejection of an electron. However, their molecular and electronic structure is very similar to that of their corresponding lithium salts, which justifies the analysis of the chemical bonding of these doubly charged systems, as it is not affected by the presence of a lithium cation.

Finally, the metalloaromaticity<sup>57</sup> of these clusters was evaluated at the BLYP/aug-cc-pVDZ level of theory with the optimized BLYP-D3(BJ)/TZ2P geometries by means of multicentre electron sharing indices (MCIs).<sup>58–60</sup> MCIs provide a measure of electron sharing among the atoms considered,<sup>59</sup> in the present case the six atoms that form each of the clusters studied. MCI values have been calculated using the ESI-3D program.<sup>61,62</sup>

## Results and discussion

We first focus on the homoatomic  $\text{X}_6^{2-}$  metal clusters with  $\text{X} = \text{B}$ ,  $\text{Al}$ , and  $\text{Ga}$ . The optimized  $O_h$  and  $D_{2h}$  geometries at the BLYP-D3(BJ)/TZ2P level are depicted in Fig. 1 with the main bond lengths and angles. As expected, B–B bond lengths (1.536–1.768 Å) are much shorter than those for Al–Al (2.574–2.912 Å) and Ga–Ga (2.526–2.898 Å). The similar Al–Al and Ga–Ga distances in  $\text{X}_6^{2-}$  metal clusters ( $\text{X} = \text{Al}$ ,  $\text{Ga}$ ) are not unexpected given the similar van der Waals radii of these two elements.<sup>63</sup> In addition, the X–X bond length connecting the two equivalent  $\text{X}_3^-$  fragments in  $O_h$  clusters is longer than in the  $D_{2h}$  systems.

Table 1 encloses the energy differences between  $O_h$  and  $D_{2h}$  clusters. For  $\text{B}_6^{2-}$   $D_{2h}$  symmetry is more stable than  $O_h$  by 67.5  $\text{kcal mol}^{-1}$ , the latter not being a minimum.<sup>18</sup> Meanwhile the opposite trend is obtained in the other two metal clusters, for which  $O_h$  is lower in energy by 15.8 ( $\text{Al}_6^{2-}$ ) and 9.3  $\text{kcal mol}^{-1}$  ( $\text{Ga}_6^{2-}$ ) than  $D_{2h}$  structures. These trends are confirmed by higher level CCSD(T)/aug-cc-pVTZ single point energy calculations at the same BLYP-D3(BJ)/TZ2P geometries (values also enclosed in

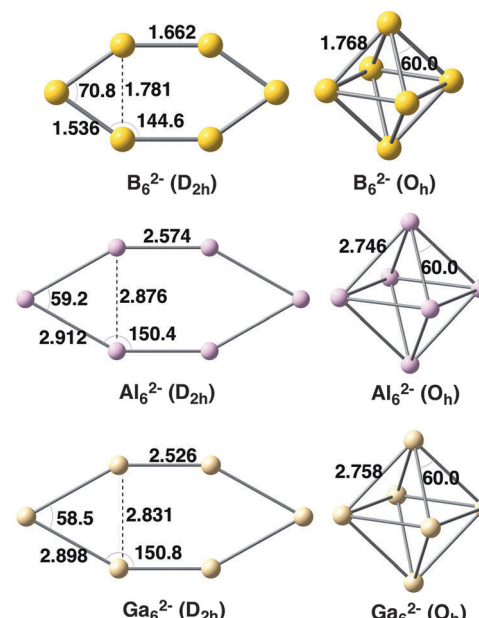


Fig. 1 Geometries of  $\text{X}_6^{2-}$  metal clusters analysed with  $D_{2h}$  and  $O_h$  symmetries. Distances in Å and angles in degrees.

Table 1 Relative energies of clusters between  $O_h$  and  $D_{2h}$  symmetries (in  $\text{kcal mol}^{-1}$ ), and the aromatic MCI criterion

Clusters	BLYP-D3(BJ)/TZ2P <sup>a</sup>		CCSD(T)/aug-cc-pVTZ <sup>b</sup>		MCI <sup>c</sup>	
	$O_h$	$D_{2h}$	$O_h$	$D_{2h}$	$O_h$	$D_{2h}$
$\text{X}_6^{2-}$						
$\text{B}_6^{2-}$	67.5 <sup>e</sup>	0.0 <sup>d</sup>	38.7	0.0	0.062	–0.052
$\text{Al}_6^{2-}$	0.0 <sup>d</sup>	15.8 <sup>e</sup>	0.0	44.8	0.077	0.068
$\text{Ga}_6^{2-}$	0.0 <sup>f</sup>	9.3 <sup>f</sup>	0.0	46.6	0.083	0.071

Clusters	BLYP-D3(BJ)/TZ2P <sup>a</sup>		CCSD(T)/aug-cc-pVTZ <sup>b</sup>		MCI <sup>c</sup>	
	$D_{4h}$	$D_{2h}$	$D_{4h}$	$D_{2h}$	$D_{4h}$	$D_{2h}$
$\text{X}_2\text{Y}_4^{2-}$						
$\text{B}_2\text{Al}_4^{2-}$	0.0 <sup>g</sup>	15.9 <sup>g</sup>	0.0	34.0	0.032	0.001
$\text{Al}_2\text{B}_4^{2-}$	66.9 <sup>h</sup>	0.0 <sup>g</sup>	48.7	0.0	0.032	0.023
$\text{Al}_2\text{Ga}_4^{2-}$	0.0 <sup>d</sup>	13.0 <sup>h</sup>	0.0	43.3	0.077	0.068
$\text{Ga}_2\text{B}_4^{2-}$	79.4 <sup>g</sup>	0.0 <sup>g</sup>	47.1	0.0	0.047	0.042
$\text{Ga}_2\text{Al}_4^{2-}$	0.0 <sup>d</sup>	14.8 <sup>g</sup>	0.0	48.2	0.074	0.072

Clusters	BLYP-D3(BJ)/TZ2P <sup>a</sup>		CCSD(T)/aug-cc-pVTZ <sup>b</sup>		MCI <sup>c</sup>	
	$D_{3h}$	$C_{3v}$	$D_{3h}$	$C_{3v}$	$D_{3h}$	$C_{3v}$
$\text{X}_3\text{Y}_3^{2-}$	0.0 <sup>d</sup>	13.2 <sup>h</sup>	0.0	45.3	0.078	0.068
$\text{Al}_3\text{Ga}_3^{2-}$						

<sup>a</sup>  $\text{B}_2\text{Ga}_4^{2-}$  ( $D_{2h}$ ) has not been obtained because optimization breaks the symmetry; whereas  $\text{B}_3\text{Al}_3^{2-}$  and  $\text{B}_3\text{Ga}_3^{2-}$  ( $O_h$ ) have not been obtained because the strength of the  $\text{B}_3$  unit causes the systems to be planar and to avoid a 3D geometry. <sup>b</sup> Single point energy calculations at BLYP-D3(BJ)/TZ2P geometries. <sup>c</sup> MCI calculated at the BLYP/aug-cc-pVDZ level of theory with the BLYP-D3(BJ)/TZ2P optimized geometries. <sup>d</sup> Local minima. <sup>e</sup> One imaginary frequency. <sup>f</sup> One small imaginary frequency due to numerical integration problems. <sup>g</sup> Two imaginary frequencies. <sup>h</sup> Three imaginary frequencies.

Table 1). The relative energies of  $\text{B}_6^{2-}$ ,  $\text{Al}_6^{2-}$ , and  $\text{Ga}_6^{2-}$  between  $O_h$  and  $D_{2h}$  symmetries are now –38.7, +44.8 and +46.6  $\text{kcal mol}^{-1}$ , respectively. CCSD(T) values systematically favour  $O_h$  as compared



to  $D_{2h}$  structures by about 20–30 kcal mol<sup>−1</sup>. However, the qualitative picture remains the same.

The aromaticity of these  $X_6^{2-}$  metal clusters was evaluated by means of the MCI electronic criterion. The six-membered MCIs are enclosed in Table 1. In all cases, the  $O_h$  system is more aromatic than the  $D_{2h}$  one, in agreement with the larger electronic delocalisation of the former, as discussed in the Introduction.<sup>21</sup> MCI values confirm the octahedral aromaticity<sup>21</sup> of  $O_h$   $Al_6^{2-}$  and the antiaromatic character of  $D_{2h}$   $B_6^{2-}$ .<sup>17,18,22,23</sup> Interestingly, MCI values point out the clear aromatic character of all 3D clusters that do not contain boron (MCI = 0.074–0.077); whereas mixed  $B_2Al_4^{2-}$ ,  $Al_2B_4^{2-}$ , and  $Ga_2B_4^{2-}$   $D_{4h}$  clusters containing boron atoms are less aromatic (MCI = 0.032–0.047). For planar structures, there are basically two groups of clusters. First, the group formed by  $B_6^{2-}$  and  $B_2Al_4^{2-}$  has eight valence electrons distributed in two  $\pi$ -MOs and two  $\sigma$ -MOs (*vide infra*). Therefore, having four  $\pi$ -electrons and four  $\sigma$ -electrons, they are  $\sigma$ - and  $\pi$ -antiaromatic species. Second, the group formed by  $Al_6^{2-}$ ,  $Ga_6^{2-}$ ,  $Al_2B_4^{2-}$ ,  $Al_2Ga_4^{2-}$ ,  $Ga_2B_4^{2-}$ , and  $Ga_2B_4^{2-}$  have eight valence electrons distributed in one  $\pi$ -MO and three  $\sigma$ -MOs (*vide infra*) and, therefore, they are  $\sigma$ - and  $\pi$ -aromatic species.

With the aim to obtain a deeper insight into the origin of 2D to 3D relative energies an energy decomposition analysis was performed, following the reaction presented in Scheme 1. As pointed out above, both systems can be constructed from two identical  $X_3^-$  anionic fragments, both in their quintet state in order to form the corresponding new bonds. Three of these bonds are of  $\sigma$  character, two tangential ( $\sigma^T$ ) and one radial ( $\sigma^R$ ), and one  $\pi$  character (see Fig. 2). It must be pointed out that, very recently, Mercero *et al.* have proven the multiconfigurational character of some of the lowest-lying electronic states of  $Al_3^-$ .<sup>19</sup> In the case of the quintet state of  $Al_3^-$ , which is the fragment

used in our calculations, the authors showed that the electronic configuration of the four valence electrons is also derived from the occupation of two  $\sigma$ -type tangential and one  $\sigma$ -type radial molecular orbitals arising from the  $3p_x$  and  $3p_y$  atomic orbitals, and one  $\pi$ -type orbital arising from the  $3p_z$  ones. This quintet state was found to be dominated by one-single configuration with a coefficient of 0.92 in the multiconfigurational wavefunction.<sup>19</sup> Moreover, the energy difference between the ground state and the quintet state was almost the same when computed at DFT or at the MCSCF levels of theory.<sup>19</sup> This seems to indicate that DFT methods give reasonable results for this quintet state. Finally, the  $T_1$  test<sup>64</sup> applied to clusters collected in Table 1 was found to be always less than 0.045, thus indicating the relatively low multiconfigurational character of these species. It is commonly accepted that CCSD(T) produces acceptable results for  $T_1$  values as high as 0.055.<sup>65</sup>

The different terms of the EDA for  $B_6^{2-}$ ,  $Al_6^{2-}$ , and  $Ga_6^{2-}$  clusters are enclosed in Table 2. First we notice that the total bonding energies ( $\Delta E$ ) are much larger for  $B_6^{2-}$  than for  $Al_6^{2-}$  or  $Ga_6^{2-}$ . For the former,  $\Delta E$  are  $-100.2$  ( $O_h$ ) and  $-179.5$  kcal mol<sup>−1</sup> ( $D_{2h}$ ), whereas for the two latter are in between  $-19.0$  and  $-38.1$  kcal mol<sup>−1</sup>. This trend correlates with the shorter B–B bond lengths mentioned above. Table 2 also encloses the relative EDA energies between the two clusters. The  $B_3^-$  fragment taken from the  $B_6^{2-}$  system in its  $D_{2h}$  symmetry is the one that suffers the largest deformation, *i.e.* the largest change in geometry with respect to the fully relaxed  $B_3^-$  cluster in the quintet state ( $\Delta E_{\text{dist}} = 12.5$  kcal mol<sup>−1</sup>), whereas the rest of the systems present small values of  $\Delta E_{\text{dist}}$  (0.0–1.7 kcal mol<sup>−1</sup>). However, differences in  $\Delta E$  are not due to distortion energies (indeed  $\Delta E_{\text{dist}}$  values follow the opposite trend as  $\Delta E$ ), but to interaction energies ( $\Delta E_{\text{int}}$ ).

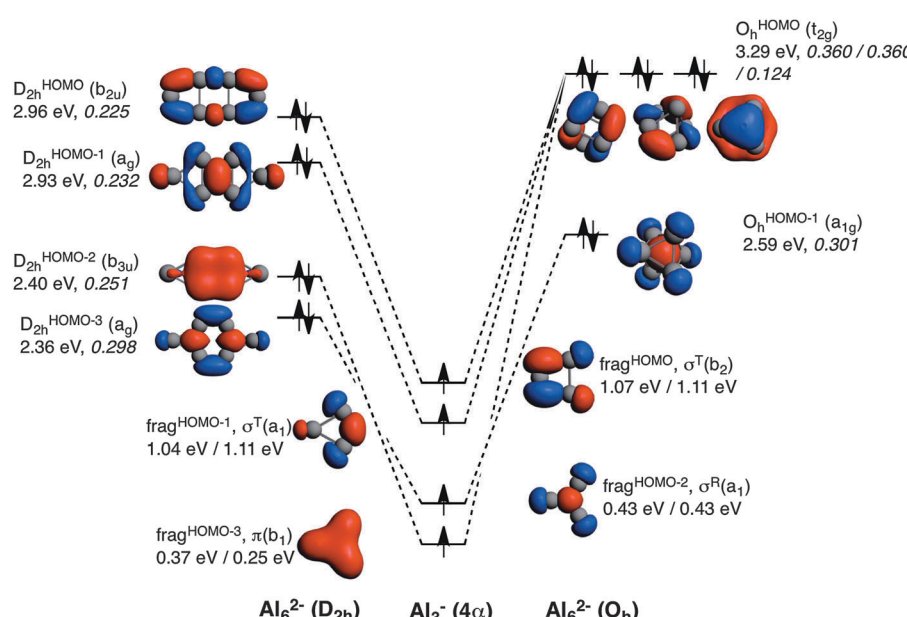


Fig. 2 Molecular orbital diagram corresponding to the formation of  $Al_6^{2-}$  in  $D_{2h}$  and  $O_h$  symmetries from two  $Al_3^-$  fragments in their quintet state. Energies of the molecular orbitals are enclosed (in eV), as well as the  $\langle \text{SOMO} | \text{SOMO} \rangle$  overlaps of the fragments (values in italics). Energies of the fragments obtained from both  $D_{2h}$  (left) and  $O_h$  (right) symmetries are also enclosed.



**Table 2** Energy decomposition analysis (EDA) of  $X_6^{2-}$  ( $X = B$ ,  $Al$ , and  $Ga$ ) metal clusters with  $D_{2h}$  and  $O_h$  symmetries (in  $\text{kcal mol}^{-1}$ ), from two  $X_3^-$  fragments in their quintet state, computed at the BLYP-D3(BJ)/TZ2P level

$B_6^{2-}$	$Al_6^{2-}$			$Ga_6^{2-}$					
	$D_{2h} + D_{2h} \rightarrow D_{2h}$	$O_h + O_h \rightarrow O_h$	$\Delta(\Delta E)$	$D_{2h} + D_{2h} \rightarrow D_{2h}$	$O_h + O_h \rightarrow O_h$	$\Delta(\Delta E)$	$D_{2h} + D_{2h} \rightarrow D_{2h}$	$O_h + O_h \rightarrow O_h$	$\Delta(\Delta E)$
$\Delta E_{\text{int}}$	-192.0	-101.4	-90.6	-20.7	-39.8	19.1	-19.1	-31.0	11.9
$\Delta E_{\text{Pauli}}$	533.5	735.3	-201.8	225.7	348.0	-122.3	269.6	384.5	-114.9
$\Delta V_{\text{elstat}}$	-239.0	-291.9	52.9	-96.3	-166.5	70.2	-138.0	-207.5	69.5
$\Delta E_{\text{oi}}$	-483.4	-542.8	59.4	-146.9	-217.4	70.5	-146.7	-203.4	56.7
$\Delta E_{\text{disp}}$	-3.2	-2.1	-1.1	-3.2	-3.9	0.7	-4.0	-4.7	0.6
$\Delta E_{\text{dist}}$	12.5	1.3	11.2	0.0	1.7	-1.7	0.1	1.4	-1.3
$\Delta E$	-179.5	-100.2	-79.3	-20.7	-38.1	17.4	-19.0	-29.6	10.6

Thus, we focus on the decomposition of  $\Delta E_{\text{int}}$  into  $\Delta E_{\text{Pauli}}$ ,  $\Delta V_{\text{elstat}}$ ,  $\Delta E_{\text{oi}}$ , and  $\Delta E_{\text{disp}}$  terms. As a general trend, in all three  $X_6^{2-}$  clusters  $\Delta E_{\text{Pauli}}$  is larger for the  $O_h$  than the  $D_{2h}$  cluster ( $\Delta(\Delta E_{\text{Pauli}}) = -201.8$ ,  $-122.3$ , and  $-114.9 \text{ kcal mol}^{-1}$  for  $B_6^{2-}$ ,  $Al_6^{2-}$ , and  $Ga_6^{2-}$ , respectively), so making it less stable. The overlaps between doubly occupied MOs are larger in the more compact  $O_h$  structure that, consequently, has larger  $\Delta E_{\text{Pauli}}$ . The larger difference in  $\Delta E_{\text{Pauli}}$  between the  $O_h$  and  $D_{2h}$  structures in the case of  $B_6^{2-}$  as compared to  $Al_6^{2-}$  and  $Ga_6^{2-}$  is attributed to the particularly short B–B distances that increase the overlap between doubly occupied MOs of each  $B_3^-$  fragment. At the same time, the  $O_h$  form presents larger (more negative) electrostatic interactions ( $\Delta(\Delta V_{\text{elstat}}) = 52.9$ ,  $70.2$ , and  $69.5 \text{ kcal mol}^{-1}$  for  $B_6^{2-}$ ,  $Al_6^{2-}$ , and  $Ga_6^{2-}$ , respectively). It is usually the case that higher destabilising Pauli repulsions go with larger stabilising electrostatic interactions. The reason has to be found in the fact that both interactions increase in the absolute value when electrons and nuclei are confined in a relatively small space. The electrostatic interaction together with orbital interaction ( $\Delta(\Delta E_{\text{oi}}) = 59.4$ ,  $70.5$ , and  $56.7 \text{ kcal mol}^{-1}$  for  $B_6^{2-}$ ,  $Al_6^{2-}$ , and  $Ga_6^{2-}$ , respectively) terms favour the  $O_h$  structure. However, in the case of  $O_h$   $B_6^{2-}$ ,  $\Delta(\Delta V_{\text{elstat}})$  and  $\Delta(\Delta E_{\text{oi}})$  cannot compensate  $\Delta(\Delta E_{\text{Pauli}})$ , which causes the  $D_{2h}$  system to be the lowest in energy. The opposite occurs for  $Al_6^{2-}$  and  $Ga_6^{2-}$ . Finally, the dispersion term almost does not affect the relative energies, as the difference in dispersion is only in the order of *ca.*  $1.0 \text{ kcal mol}^{-1}$ . Therefore, what causes the different trend observed for  $B_6^{2-}$  on one side, and  $Al_6^{2-}$  and  $Ga_6^{2-}$  on the other side is basically the  $\Delta E_{\text{oi}}$  term, which combined with the  $\Delta V_{\text{elstat}}$  component does ( $Al_6^{2-}$  and  $Ga_6^{2-}$ ) or does not ( $B_6^{2-}$ ) compensate the higher  $\Delta E_{\text{Pauli}}$  of the  $O_h$  form.

The comparison of the MOs diagrams of  $B_6^{2-}$  and  $Al_6^{2-}$ , built from their  $X_3^-$  fragments, justify the trends of  $\Delta E_{\text{oi}}$  (see Fig. 2 and 3). Both  $D_{2h}$  and  $O_h$  clusters are built from the same fragments; the only difference is that the two tangential  $\text{frag}^{\text{HOMO}}(\sigma^T(b_2))$  and  $\text{frag}^{\text{HOMO-1}}(\sigma^T(a_1))$  MOs of  $Al_3^-$  are degenerate when obtained from  $Al_6^{2-}$  in its  $O_h$  geometry, whereas they are not when generated from the  $D_{2h}$  system, although they still are very close in energy. As discussed from the EDA,  $O_h$  is more stable than  $D_{2h}$  because of more stabilizing electrostatic and orbital interactions, which compensate its larger Pauli repulsion. Fig. 2 also encloses the overlaps for the interactions between the four SOMOs of the  $Al_3^-$  fragments to form the MOs of the metal clusters in both geometries.

We take the  $Al_3^-$  fragments in their quintet states with three unpaired  $\sigma$ - and one unpaired  $\pi$ -electrons, all of them with spin  $\alpha$  in one fragment and  $\beta$  in the other. A more negative  $\Delta E_{\text{oi}}$  in  $O_h$   $Al_6^{2-}$  is justified from the larger  $\langle \text{SOMO} | \text{SOMO} \rangle$  overlaps, especially for  $t_{2g} O_h^{\text{HOMO}a}$  and  $O_h^{\text{HOMO}b}$  (0.360 compared to 0.225 and 0.232 for  $b_{2u} D_{2h}^{\text{HOMO}}$  and  $a_g D_{2h}^{\text{HOMO-1}}$ , respectively).  $D_{2h}$  only presents a larger overlap for the  $\pi$  fragment orbital (0.251 for  $b_{3u} D_{2h}^{\text{HOMO-2}}$  and 0.124 for  $t_{2g} O_h^{\text{HOMO}c}$ ). Meanwhile both of them have almost the same overlap for the combination of the radial MO ( $\sigma^R$ ) fragment ( $\text{frag}^{\text{HOMO-2}}$ ), with  $\langle \text{SOMO} | \text{SOMO} \rangle = 0.298$  and 0.301 for  $a_g D_{2h}^{\text{HOMO-3}}$  and  $O_h^{\text{HOMO-1}}$ , respectively. Overall, the higher orbital interaction term of the  $O_h$  system can be explained by the larger  $\langle \text{SOMO} | \text{SOMO} \rangle$  overlaps of two of the  $t_{2g}$  delocalised molecular orbitals for this cluster (see Fig. 2). The energies of the occupied MOs of  $Al_6^{2-}$  formed are higher than those of the  $Al_3^-$  SOMOs because we move from a mono-anionic fragment to a dianionic molecule.

Now it is the turn to visualize the MOs of  $B_6^{2-}$ . The fragments for  $B_3^-$  are the same as those for  $Al_3^-$  (see Fig. 3). However, the first difference appears in the MOs for  $B_6^{2-}$  with  $D_{2h}$  symmetry. In this case, it would be more reasonable to build the MOs of this molecule from two triplet (not quintet)  $B_3^-$  fragments. The reason is the different occupation of the MOs when compared to the  $D_{2h}$   $Al_6^{2-}$  species. In  $D_{2h} B_6^{2-}$ , the HOMO corresponds to the antibonding  $\pi$  MO. To reach doubly occupied bonding ( $b_{3u} D_{2h}^{\text{HOMO-4}}$ ) and antibonding ( $b_{2g} D_{2h}^{\text{HOMO}}$ )  $\pi$  MOs, the  $\pi$  MO ( $\text{frag}^{\text{HOMO-3}}$ ) should be doubly occupied. Furthermore, the tangential  $\sigma^T(a_1)$   $\text{frag}^{\text{HOMO}}$  does not participate in any occupied MO of this metal cluster and only generates virtual MOs. Consequently, MOs of  $B_6^{2-}$  are better formed from two  $B_3^-$  fragments in their triplet state (see red electron in Fig. 3). On the other hand,  $B_6^{2-}$  with  $O_h$  follows the same trend as  $Al_6^{2-}$ , and in this case the same SOMOs in their quintet state are involved. At this point, it is worth mentioning that, as pointed out by Mercero *et al.*, due to the strong multiconfigurational character of this species, one must be cautious with the electronic configuration, especially for the triplet state, as radial and tangential MOs are very close in energy.<sup>19</sup>

To make results comparable, Table 2 gathers the EDA of  $O_h$  and  $D_{2h}$   $B_6^{2-}$  from two  $B_3^-$  fragments in their quintet states. Also in this case  $\Delta E_{\text{oi}}$  is more favourable for  $O_h$  than for  $D_{2h}$ , however, at a lower extent when compared to  $Al_6^{2-}$ . There are two main reasons for such a decrease of the strength of  $\Delta E_{\text{oi}}$  in  $O_h$  compared to  $D_{2h}$ . First, and more importantly, because



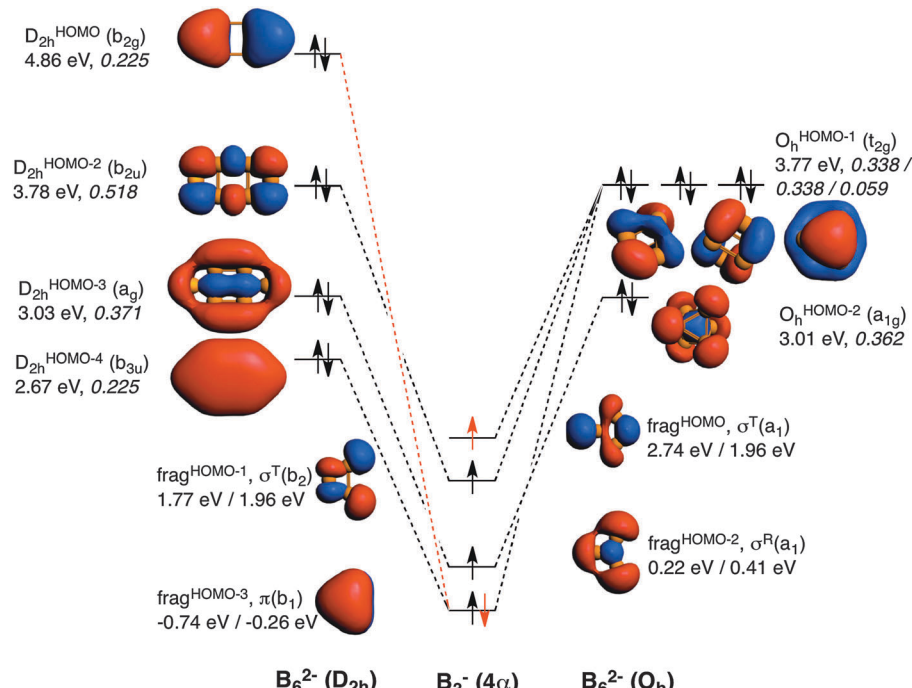


**Fig. 3** Molecular orbital diagram corresponding to the formation of  $B_6^{2-}$  in  $D_{2h}$  and  $O_h$  symmetries from two  $B_3^-$  fragments in their quintet states. Electrons in red refer to the formation of  $B_6^{2-}$  ( $D_{2h}$ ) from  $B_3^-$  fragments in their triplet state. In the triplet state,  $\pi(b_1)$  is doubly occupied,  $\sigma^R(a_1)$  and  $\sigma^T(b_2)$  remain singly occupied, and the  $\sigma^T(a_1)$  becomes unoccupied. Energies of the molecular orbitals are enclosed (in eV), as well as the  $\langle \text{SOMO} | \text{SOMO} \rangle$  overlaps of the fragments (values in italics). Energies of the fragments obtained from both  $D_{2h}$  (left) and  $O_h$  (right) symmetries are also enclosed.

the  $D_{2h}^{\text{HOMO-2}}$  formed presents a much larger  $\langle \text{SOMO} | \text{SOMO} \rangle$  overlap than  $t_{2g} O_h^{\text{HOMO-1}}$  (0.518 in the former vs. 0.338 in the latter). In particular, this  $D_{2h}^{\text{HOMO-2}}$  MO contributes to the 2c-2e B-B localised bonds that are related to the larger covalent character of this structure. And second, because the  $\pi$ -interaction between the two  $\pi$  SOMO fragments is much larger in the case of  $D_{2h}$  (0.225 vs. 0.059 for  $D_{2h}$  and  $O_h$ , respectively). Nevertheless, these two more favourable orbital interactions are not enough to surpass the  $\Delta E_{\text{oi}}$  term of the  $O_h$  cluster. However, as compared to  $\text{Al}_6^{2-}$ , for  $B_6^{2-}$  the  $\Delta(\Delta E_{\text{oi}})$  term favours the  $O_h$  system to a less extent and cannot compensate the higher  $\Delta E_{\text{Pauli}}$  term of the  $O_h$  form, thus making the planar geometry to be more stable in this case. This is related to the determinant force of the formed covalent bonding, involving more localised MOs than for  $\text{Al}_6^{2-}$ . Such a larger covalent component in  $B_6^{2-}$  is also supported by the covalent character of the interaction between the two fragments calculated as % covalency =  $(\Delta E_{\text{oi}} / (\Delta E_{\text{oi}} + \Delta V_{\text{elstat}} + \Delta E_{\text{disp}})) \times 100$ . This formula results in  $B_6^{2-}$ : 65–67% ( $O_h$ ,  $D_{2h}$ ),  $\text{Al}_6^{2-}$ : 56–60% ( $O_h$ ,  $D_{2h}$ ), and  $\text{Ga}_6^{2-}$ : 49–51% ( $O_h$ ,  $D_{2h}$ ); thus confirming again the larger covalency found in  $B_6^{2-}$ .

Finally, as done usually in the turn-upside-down approach,<sup>36–39,56,66,67</sup> instead of building  $X_6^{2-}$  in  $O_h$  symmetry from the corresponding two  $X_3^-$  fragments obtained from the  $O_h$  structure, we can build the  $O_h$  system from two  $X_3^-$  fragments extracted from the  $X_6^{2-}$  cluster in  $D_{2h}$  symmetry, and viceversa (see Tables S2–S4 in the ESI<sup>†</sup>). The main conclusions remain unaltered and confirm that the  $D_{2h}$  structures suffer a lower Pauli repulsion whereas those of  $O_h$  symmetry have more favourable electrostatic and orbital interactions. The interplay

between the Pauli repulsion on the one hand and electrostatic and orbital interactions on the other determines the most favourable symmetry in each case.

Just to conclude this section, we must point out that the whole EDA and turn-upside-down analyses were performed with fragments in their quintet state. However, as we commented before this is not the most reasonable way to build  $B_6^{2-}$  in  $D_{2h}$  symmetry. Table S5 (ESI<sup>†</sup>) contains the EDA for  $O_h$  and  $D_{2h}$   $B_6^{2-}$  systems using  $B_3^-$  fragments in their triplet states. Results show that although the different terms are larger in the absolute value, the trends discussed above are not affected, and the  $D_{2h}$  cluster is favoured mainly because of smaller Pauli repulsions.

### Mixed metal clusters

In this section, we analyse the  $X_2Y_4^{2-}$  clusters with  $X, Y = \text{B}, \text{Al}, \text{Ga}$  and  $X \neq Y$  (see Fig. 4). The relative energies of the planar and 3D forms are also enclosed in Table 1. In all cases, the  $D_{2h}$  system is preferred when the cluster incorporates four B atoms; otherwise the 3D  $D_{4h}$  geometry is the lowest in energy. In particular, the  $D_{2h}$  symmetry is much more stable for  $\text{Al}_2\text{B}_4^{2-}$  and  $\text{Ga}_2\text{B}_4^{2-}$  by 66.9 and 79.4 kcal mol<sup>-1</sup>, respectively. On the other hand, when B is not the predominant atom, the  $D_{4h}$  cluster is more stable by about 9–16 kcal mol<sup>-1</sup>. As for the homoatomic metal clusters, at the CCSD(T) level, the same trend is obtained, although the  $D_{4h}$  system is stabilized with respect to the  $D_{2h}$  one by 20–30 kcal mol<sup>-1</sup>. It is important to note that the  $D_{4h}$  and  $D_{2h}$  systems are not always the most stable for the  $X_2Y_4^{2-}$  clusters. For instance, for  $\text{Al}_2\text{B}_4^{2-}$ , a  $C_2$  geometry is the most stable form and, for  $\text{B}_2\text{Al}_4^{2-}$ , a  $C_{2v}$  structure is the

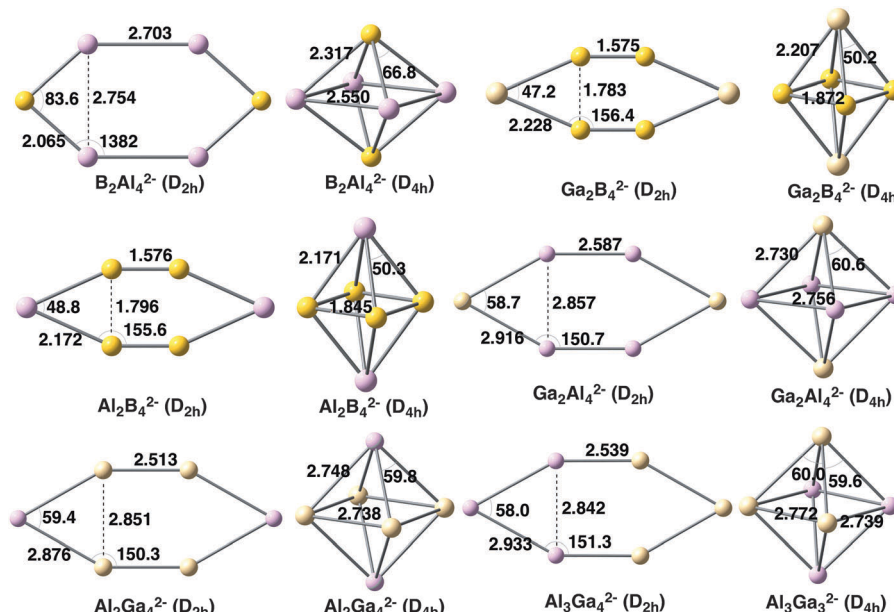


Fig. 4 Geometries of mixed metal clusters analysed with planar and 3D geometries. Distances in Å and angles in degrees.

lowest in energy.<sup>18</sup> However, we are not interested here in finding the most stable structure for each cluster but to discuss the reasons why in some cases 2D clusters are preferred over 3D and the other way round. Finally,  $\text{Al}_3\text{Ga}_3^{2-}$  also prefers an  $O_h$  geometry by 13.2 kcal mol<sup>-1</sup>. Unfortunately, this latter relative energy cannot be compared to those of  $\text{B}_3\text{Al}_3^{2-}$  or  $\text{B}_3\text{Ga}_3^{2-}$  because the strength of the localised bonding between three B atoms prevents the optimization of their 3D structures. In this context, it is worth mentioning that Alexandrova and coworkers<sup>26</sup> found in  $\text{X}_3\text{Y}_3$  ( $\text{X} = \text{B}, \text{Al}, \text{Ga}; \text{Y} = \text{P}, \text{As}$ ) clusters that the lighter

elements prefer 2D structures, whereas the heavier ones favour 3D geometries.

The EDA was also performed for this series of six mixed metal clusters (see Table 3) with the aim to further understand the determinant force towards the most stable cluster. For the  $\text{X}_2\text{Y}_4^{2-}$  clusters, the EDA was carried out taken  $\text{YXY}^-$  fragments in their quintet states. For  $\text{Al}_3\text{Ga}_3^{2-}$ , the fragments were  $\text{Al}_3^-$  and  $\text{Ga}_3^-$  in the quintet state too. For those systems for which the out-of-plane geometry is the most stable, the combination of more favourable electrostatic and orbital interactions, even though presenting larger Pauli repulsion, gives the explanation to the trend observed. This is the same behaviour already discussed above for both  $\text{Al}_6^{2-}$  and  $\text{Ga}_6^{2-}$  systems. On the other hand, when  $D_{2h}$  symmetry is the cluster lower in energy, as for  $\text{Al}_2\text{B}_4^{2-}$  and  $\text{Ga}_2\text{B}_4^{2-}$  metal clusters, even though the  $D_{4h}$  system presents more stable electrostatic interaction, now the orbital interactions in combination with less unfavourable Pauli repulsion favour the  $D_{2h}$  symmetry. This latter behaviour differs from that of  $\text{B}_6^{2-}$ , for which the orbital interactions also favour the  $O_h$  symmetry, thus making Pauli repulsion the determinant factor towards the preference for planar  $D_{2h}$   $\text{B}_6^{2-}$ .

## Conclusions

In previous studies,<sup>18</sup> the preference of  $\text{B}_6^{2-}$  for the planar  $D_{2h}$  geometry and of  $\text{Al}_6^{2-}$  for the 3D  $O_h$  one was justified by the inclination for localised covalent bonding in the former cluster and delocalised bonding in the latter. These two effects point in opposite directions. In the present work, we go one-step further by showing that the preference of  $\text{B}_6^{2-}$  for the planar  $D_{2h}$  form is due to two particular molecular orbital interactions. From one side the  $D_{2h}^{\text{HOMO}-1}(\text{b}_{2u})$  formed from two tangential SOMO  $\sigma^T(\text{b}_2)$  orbitals. This orbital is related to localised covalent

Table 3 Energy decomposition analysis (EDA) of all mixed metal clusters with planar and 3D symmetries (in kcal mol<sup>-1</sup>), from two fragments at their quintet states, computed at the BLYP-D3(BJ)/TZ2P level

		$\Delta E_{\text{int}}$	$\Delta E_{\text{Pauli}}$	$\Delta V_{\text{elstat}}$	$\Delta E_{\text{oi}}$	$\Delta E_{\text{disp}}$
$\text{B}_2\text{Al}_4^{2-}$	$D_{4h}$	-52.1	440.1	-202.7	-285.7	-3.9
	$D_{2h}$	-40.4	243.4	-98.1	-182.5	-3.3
	$\Delta E$	11.7	-196.7	104.6	103.2	0.6
$\text{Al}_2\text{B}_4^{2-}$	$D_{4h}$	-75.1	584.0	-251.7	-404.1	-3.3
	$D_{2h}$	-139.6	556.6	-238.6	-454.5	-3.3
	$\Delta E$	-64.6	-27.4	13.2	-50.4	0.0
$\text{Al}_2\text{Ga}_4^{2-}$	$D_{4h}$	-35.0	381.2	-201.0	-210.6	-4.6
	$D_{2h}$	-19.2	283.1	-147.1	-151.4	-3.8
	$\Delta E$	15.8	-98.1	53.8	59.3	0.8
$\text{Ga}_2\text{B}_4^{2-}$	$D_{4h}$	-83.8	590.4	-262.5	-408.2	-3.5
	$D_{2h}$	-157.5	540.0	-225.6	-468.6	-3.2
	$\Delta E$	-73.7	-50.4	36.8	-60.4	0.3
$\text{Ga}_2\text{Al}_4^{2-}$	$D_{4h}$	-38.4	370.1	-188.0	-216.1	-4.3
	$D_{2h}$	-20.6	218.0	-90.8	-144.4	-3.6
	$\Delta E$	17.8	-152.0	97.3	71.7	0.8
$\text{Al}_3\text{Ga}_3^{2-}$	$D_{3h}$	-36.8	381.0	-197.8	-215.7	-4.2
	$C_{3v}$	-20.7	254.4	-122.8	-148.7	-3.6
	$\Delta E$	16.1	-126.6	75.0	67.0	0.6



bonding, and has a much more important weight in  $B_6^{2-}$  than in  $Al_6^{2-}$ , proving the dominant localised covalent character in the former. And the second determinant interaction is that of  $\pi$  character. In the case of  $O_h^{HOMO-1}(t_{2g})$  for  $B_6^{2-}$ , its formation from two  $\pi$  SOMO orbitals is much less favourable than for  $Al_6^{2-}$ . This result is in line with a dominant delocalisation force in Al clusters and more localised bonding in B metal clusters. For mixed clusters, we have found that those with more than two B atoms prefer the planar structure for same reasons discussed for  $B_6^{2-}$ .

## Acknowledgements

This work was supported by the Ministerio de Economía y Competitividad (MINECO) of Spain (Project CTQ2014-54306-P) and the Generalitat de Catalunya (project 2014SGR931, Xarxa de Referència en Química Teòrica i Computacional, ICREA Academia 2014 prize for M.S., and grant No. 2014FI\_B\_00429 to O. E. B.). The EU under the FEDER grant UNGI10-4E-801 (European Fund for Regional Development) has also funded this research. J. P. thanks the National Research School Combination-Catalysis (NRSC-C), and The Netherlands Organization for Scientific Research (NWO/CW and NWO/NCF). The authors are grateful to Dr Ferran Feixas for fruitful discussions.

## References

- Y. Hu, T. J. Wagener, Y. Gao, H. M. Meyer and J. H. Weaver, *Phys. Rev. B: Condens. Matter Mater. Phys.*, 1988, **38**, 3037–3044.
- B. Wang, H. Wang, H. Li, C. Zeng, J. G. Hou and X. Xiao, *Phys. Rev. B: Condens. Matter Mater. Phys.*, 2000, **63**, 035403.
- V. Torma, T. Reuter, O. Vidoni, M. Schumann, C. Radehaus and G. Schmid, *ChemPhysChem*, 2001, **2**, 546–548.
- R. N. Barnett, C. L. Cleveland, H. Häkkinen, W. D. Luedtke, C. Yannouleas and U. Landman, *Eur. Phys. J. D*, 1999, **9**, 95–104.
- S. Aldridge and A. J. Downs, *The Group 13 Metals Aluminium, Gallium, Indium and Thallium: Chemical Patterns and Peculiarities*, John Wiley & Sons, Ltd, Chichester, 2011.
- A. N. Alexandrova, K. A. Birch and A. I. Boldyrev, *J. Am. Chem. Soc.*, 2003, **125**, 10786–10787.
- A. N. Alexandrova and A. I. Boldyrev, *Inorg. Chem.*, 2004, **43**, 3588–3592.
- A. N. Alexandrova, A. I. Boldyrev, H.-J. Zhai and L.-S. Wang, *Coord. Chem. Rev.*, 2006, **250**, 2811–2866.
- H.-J. Zhai, A. N. Alexandrova, L.-S. Wang and A. I. Boldyrev, *Angew. Chem., Int. Ed.*, 2003, **42**, 6004–6008.
- A. I. Boldyrev and L.-S. Wang, *Chem. Rev.*, 2005, **105**, 3716–3757.
- A. E. Kuznetsov, K. A. Birch, A. I. Boldyrev, X. Li, H.-J. Zhai and L.-S. Wang, *Science*, 2003, **300**, 622–625.
- A. E. Kuznetsov, A. I. Boldyrev, H.-J. Zhai, X. Li and L.-S. Wang, *J. Am. Chem. Soc.*, 2002, **124**, 11791–11801.
- X. Li, A. E. Kuznetsov, H.-F. Zhang, A. Boldyrev and L.-S. Wang, *Science*, 2001, **291**, 859–861.
- A. E. Kuznetsov, A. I. Boldyrev, H.-J. Zhai, X. Li and L.-S. Wang, *J. Am. Chem. Soc.*, 2002, **124**, 11791–11801.
- O. C. Thomas, W.-J. Zheng, T. P. Lippa, S.-J. Xu, S. A. Lyapustina and K. H. Bowen, *J. Chem. Phys.*, 2001, **114**, 9895–9900.
- A. N. Alexandrova, A. I. Boldyrev, H.-J. Zhai and L.-S. Wang, *J. Chem. Phys.*, 2005, **122**, 054313.
- A. N. Alexandrova, A. I. Boldyrev, H.-J. Zhai, L.-S. Wang, E. Steiner and P. W. Fowler, *J. Phys. Chem. A*, 2003, **107**, 1359–1369.
- M. T. Huynh and A. N. Alexandrova, *J. Phys. Chem. Lett.*, 2011, **2**, 2046–2051.
- J. M. Mercero, E. Matito, F. Ruipérez, I. Infante, X. Lopez and J. M. Ugalde, *Chem. – Eur. J.*, 2015, **21**, 9610–9614.
- C. Corminboeuf, C. S. Wannere, D. Roy, R. B. King and P. v. R. Schleyer, *Inorg. Chem.*, 2006, **45**, 214–219.
- O. El Bakouri, M. Duran, J. Poater, F. Feixas and M. Solà, *Phys. Chem. Chem. Phys.*, 2016, DOI: 10.1039/c5cp07011b.
- J. Ma, Z. Li, K. Fan and M. Zhou, *Chem. Phys. Lett.*, 2003, **372**, 708–716.
- L.-M. Yang, J. Wang, Y.-H. Ding and C.-C. Sun, *Phys. Chem. Chem. Phys.*, 2008, **10**, 2316–2320.
- A. N. Alexandrova, *Chem. Phys. Lett.*, 2012, **533**, 1–5.
- A. N. Alexandrova, M. J. Nayhouse, M. T. Huynh, J. L. Kuo, A. V. Melkonian, G. Chavez, N. M. Hernando, M. D. Kowal and C.-P. Liu, *Phys. Chem. Chem. Phys.*, 2012, **14**, 14815–14821.
- A. N. Alexandrova, M. R. Nechay, B. R. Lydon, D. P. Buchan, A. J. Yeh, M.-H. Tai, I. P. Kostrikin and L. Gabrielyan, *Chem. Phys. Lett.*, 2013, **588**, 37–42.
- J. E. Fowler and J. M. Ugalde, *J. Phys. Chem. A*, 2000, **104**, 397–403.
- J. E. Fowler and J. M. Ugalde, *Phys. Rev. A: At., Mol., Opt. Phys.*, 1998, **58**, 383–388.
- P. Farràs, N. Vankova, L. L. Zeonjuk, J. Warneke, T. Dülcks, T. Heine, C. Viñas, F. Teixidor and D. Gabel, *Chem. – Eur. J.*, 2012, **18**, 13208–13212.
- M. R. Fagiani, L. Liu Zeonjuk, T. K. Esser, D. Gabel, T. Heine, K. R. Asmis and J. Warneke, *Chem. Phys. Lett.*, 2015, **625**, 48–52.
- J. K. Olson and A. I. Boldyrev, *J. Phys. Chem. A*, 2013, **117**, 1614–1620.
- K. Kitaura and K. Morokuma, *Int. J. Quantum Chem.*, 1976, **10**, 325–340.
- K. Morokuma, *Acc. Chem. Res.*, 1977, **10**, 294–300.
- T. Ziegler and A. Rauk, *Theor. Chim. Acta*, 1977, **46**, 1–10.
- T. Ziegler and A. Rauk, *Inorg. Chem.*, 1979, **18**, 1558–1565.
- M. El-Hamdi, W. Tiznado, J. Poater and M. Solà, *J. Org. Chem.*, 2011, **76**, 8913–8921.
- M. El-Hamdi, O. El Bakouri El Farri, P. Salvador, B. A. Abdelouahid, M. S. El Begrani, J. Poater and M. Solà, *Organometallics*, 2013, **32**, 4892–4903.
- M. El-Hamdi, M. Solà, G. Frenking and J. Poater, *J. Phys. Chem. A*, 2013, **117**, 8026–8034.
- R. Islas, J. Poater, E. Matito and M. Solà, *Phys. Chem. Chem. Phys.*, 2012, **14**, 14850–14859.
- G. te Velde, F. M. Bickelhaupt, E. J. Baerends, C. Fonseca Guerra, S. J. A. van Gisbergen, J. G. Snijders and T. Ziegler, *J. Comput. Chem.*, 2001, **22**, 931–967.
- A. D. Becke, *Phys. Rev. A: At., Mol., Opt. Phys.*, 1988, **38**, 3098–3100.



42 C. Lee, W. Yang and R. G. Parr, *Phys. Rev. B: Condens. Matter Mater. Phys.*, 1988, **37**, 785–789.

43 S. Grimme, J. Antony, S. Ehrlich and H. Krieg, *J. Chem. Phys.*, 2010, **132**, 154104.

44 S. Grimme, S. Ehrlich and L. Goerigk, *J. Comput. Chem.*, 2011, **32**, 1456–1465.

45 M. J. Frisch, G. W. Trucks, H. B. Schlegel, G. E. Scuseria, M. A. Robb, J. R. Cheeseman, G. Scalmani, V. Barone, B. Mennucci, G. A. Petersson, H. Nakatsuji, M. Caricato, X. Li, H. P. Hratchian, A. F. Izmaylov, J. Bloino, G. Zheng, J. L. Sonnenberg, M. Hada, M. Ehara, K. Toyota, R. Fukuda, J. Hasegawa, M. Ishida, T. Nakajima, Y. Honda, O. Kitao, H. Nakai, T. Vreven, J. A. Montgomery Jr., J. E. Peralta, F. Ogliaro, M. Bearpark, J. J. Heyd, E. Brothers, K. N. Kudin, V. N. Staroverov, R. Kobayashi, J. Normand, K. Raghavachari, A. Rendell, J. C. Burant, S. S. Iyengar, J. Tomasi, M. Cossi, N. Rega, J. M. Millam, M. Klene, J. E. Knox, J. B. Cross, V. Bakken, C. Adamo, J. Jaramillo, R. Gomperts, R. E. Stratmann, O. Yazyev, A. J. Austin, R. Cammi, C. Pomelli, J. W. Ochterski, R. L. Martin, K. Morokuma, V. G. Zakrzewski, G. A. Voth, P. Salvador, J. J. Dannenberg, S. Dapprich, A. D. Daniels, Ö. Farkas, J. B. Foresman, J. V. Ortiz, J. Cioslowski and D. J. Fox, *Gaussian 09, Revision A.02 ed.*, Gaussian, Inc., Pittsburgh, PA, 2009.

46 J. Cizek, *J. Chem. Phys.*, 1966, **45**, 4256–4266.

47 G. D. Purvis III and R. J. Bartlett, *J. Chem. Phys.*, 1982, **76**, 1910–1918.

48 K. Raghavachari, G. W. Trucks, J. A. Pople and M. Head-Gordon, *Chem. Phys. Lett.*, 1989, **157**, 479–483.

49 T. H. Dunning Jr., *J. Chem. Phys.*, 1989, **90**, 1007–1023.

50 R. A. Kendall, T. H. Dunning Jr. and R. J. Harrison, *J. Chem. Phys.*, 1992, **96**, 6796–6806.

51 F. M. Bickelhaupt and E. J. Baerends, in *Rev. Comput. Chem.*, ed. K. B. Lipkowitz and D. B. Boyd, Wiley-VCH, New York, 2000, vol. 15, pp. 1–86.

52 F. M. Bickelhaupt, A. Diefenbach, S. P. de Visser, L. J. de Koning and N. M. M. Nibbering, *J. Phys. Chem. A*, 1998, **102**, 9549–9553.

53 C. Fonseca Guerra, J.-W. Handgraaf, E. J. Baerends and F. M. Bickelhaupt, *J. Comput. Chem.*, 2004, **25**, 189–210.

54 I. Fernández and G. Frenking, *Faraday Discuss.*, 2007, **135**, 403–421.

55 I. Fernández and G. Frenking, *Chem. – Eur. J.*, 2007, **13**, 5873–5884.

56 R. Islas, J. Poater and M. Solà, *Organometallics*, 2014, **33**, 1762–1773.

57 F. Feixas, E. Matito, J. Poater and M. Solà, *Wiley Interdiscip. Rev.: Comput. Mol. Sci.*, 2013, **3**, 105–122.

58 P. Bultinck, R. Ponec and S. Van Damme, *J. Phys. Org. Chem.*, 2005, **18**, 706–718.

59 F. Feixas, E. Matito, J. Poater and M. Solà, *Chem. Soc. Rev.*, 2015, **44**, 6434–6451.

60 J. Poater, M. Duran, M. Solà and B. Silvi, *Chem. Rev.*, 2005, **105**, 3911–3947.

61 E. Matito, M. Duran and M. Solà, *J. Chem. Phys.*, 2005, **122**, 014109.

62 E. Matito, *ESI-3D: Electron Sharing Indexes Program for 3D Molecular Space Partitioning*, Institute of Computational Chemistry and Catalysis, Girona, 2006, <http://iqc.udg.es/~eduard/ESI>.

63 S. Alvarez, *Dalton Trans.*, 2013, **42**, 8617–8636.

64 T. J. Lee and P. R. Taylor, *Int. J. Quantum Chem., Quantum Chem. Symp.*, 1989, **S23**, 199–207.

65 J. M. L. Martin, in *Energetics of Stable Molecules and Reactive Intermediates*, ed. M. S. Minas da Piedade, Kluwer Academic Publishers, Dordrecht, 1999, vol. 535, pp. 373–417.

66 J. Poater, R. Visser, M. Solà and F. M. Bickelhaupt, *J. Org. Chem.*, 2007, **72**, 1134–1142.

67 E. Díaz-Cervantes, J. Poater, J. Robles, M. Swart and M. Solà, *J. Phys. Chem. A*, 2013, **117**, 10462–10469.

